Sputtering of Liquid Metal Suspended on an Insulating Reservoir by Radio Frequency Self-Bias

Magdaleno R. VASQUEZ Jr.[*], Toshiro KASUYA[*], Yasuyuki KIMURA[*],
Shuichi MAENO[**], Takahiro KENMOTSU[***] and Motoi WADA[*]

(Received March 3, 2010)

A liquid metal sputtering system equipped with a SiO_2 reservoir and a radio frequency (RF) power supply has been designed and built to minimize possible contamination due to sputtering from any materials other than the target material. An electrode fitted with cylindrical and toroidal magnets was designed and mounted at the bottom of the spherical glass chamber in order to confine the discharge near the target and enhance the ionization efficiency. The inductively coupled plasma configuration exhibited good coupling of the RF power to the gas discharge sustained at low gas pressures and high RF powers. Liquid gallium suspended upon the chamber bottom was confirmed sputtered by the surrounding plasma by a quadrupole mass analyzer. Electron temperature (T_e) was estimated from the optical emission lines under the local thermodynamic equilibrium (LTE) approximation.

Key words: RF discharges, CCP, ICP, sputtering, liquid metals

1. Introduction

Plasma-assisted processes such as sputtering of a target material have become an indispensable tool for thin film growth and surface modification especially in the semiconductor industry.[1)] Hence, in order to enhance and optimize the efficiency in the sputtering process, theoretical models of plasma-surface interactions and sheath dynamics should be considered. However, due to the complexity and difficulty of direct observation in the atomic scale, the exact prediction of plasma-surface interactions has certain limitations. Thus, experimental efforts have always been essential in the study of these processes.

Radio frequency (RF) powered sources are widely used in industry and laboratories. A RF discharge offers many advantages compared to a direct current (DC) discharge. High atomic fraction and cathode contamination-free plasma are only a few of these advantages. In order to increase sputtering efficiency and minimize sputtering at the deposition substrate, planar magnetron electrodes have been extensively utilized to confine the discharge around the target surface by means of a toroidal magnetic field produced by the permanent magnets of the electrode. Naturally, these two concepts are integrated into planar magnetron RF sputter system favorable to crystal growth of electronic materials.[2)]

Gallium nitride (GaN) formation via a plasma-sputter-type ion source system has been tested in DC plasma[3)] and in RF planar magnetron sputtering system[4)]

[*]Graduate School of Engineering, Doshisha University, Kyotanabe, Kyoto 610-0321 Japan
Telephone: +81-774-65-6349, E-mail: eti1106@mail4.doshisha.ac.jp
[**]Novelion Systems, Co., Ltd., Kyotanabe, Kyoto 610-0332 Japan
[***]Department of Biomedical Engineering, Doshisha University, Kyotanabe, Kyoto 610-0321 Japan

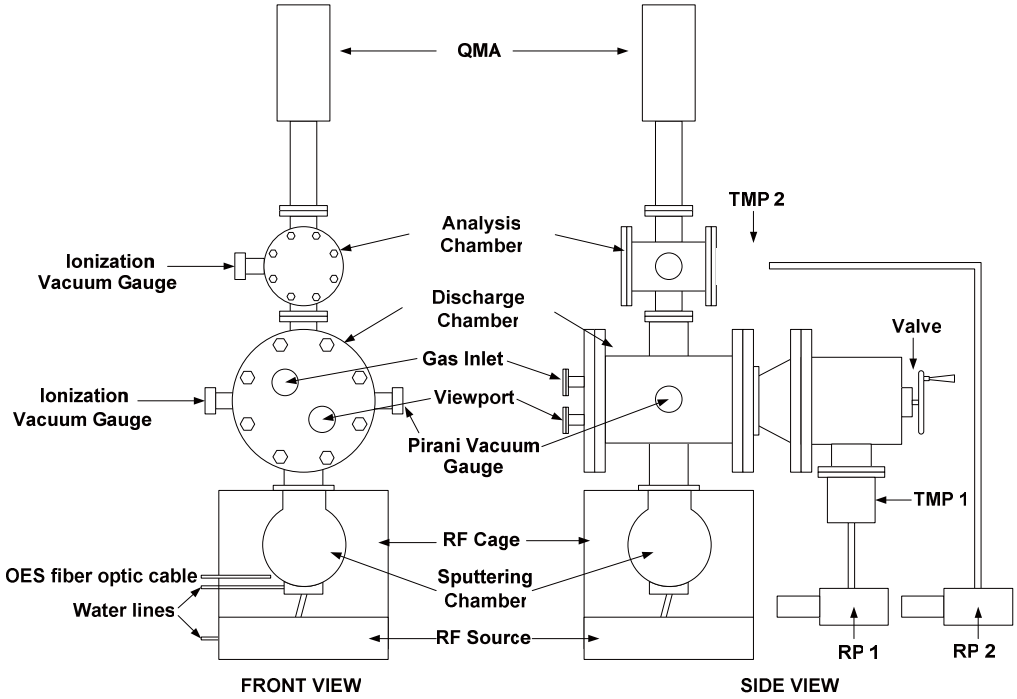

Figure 1. Schematic diagram of the sputtering system.

using liquid gallium (Ga) targets. However, these experiments utilized a metallic target holder that can contaminate the sputtered material thereby affecting the properties of the produced film. Thus, in order to minimize contamination, testing of a sputtering system with an insulating reservoir has been conceived. In this study, we present results of a sputtering system with an insulating reservoir under a RF self-bias fitted with a water-cooled magnetron electrode.

2. Experimental Set-up

A sputtering system has been designed equipped with a 120-mm diameter and 5-mm thick spherical glass chamber coupled to a 13.56 MHz RF power generator (ANELVA PRF-053B) with an auto-tuning matching box. Figure 1 shows the schematic diagram of the sputtering system. The system was divided into two chambers separated by a 2.5-mm diameter orifice. The analysis chamber was used for flux measurements while the discharge chamber was used for plasma irradiation and sputtering of a liquid metal target. Each chamber was evacuated by a turbo-molecular pump (TMP) coupled to a rotary pump (RP). A 50-mm diameter copper (Cu) electrode, shown in Fig. 2, equipped with cylindrical and toroidal magnets, was attached to the lower part of the chamber in order to confine the discharge near the target surface. The magnets form a planar magnetron geometry to enhance the local ionization due to RF field. The surface of the electrode was made spherical in order to fit and make full contact to the bottom of the glass

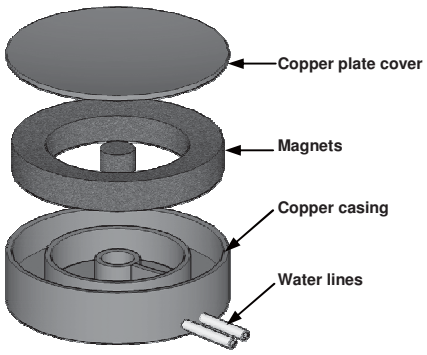

Figure 2. Expanded view of the Cu planar magnetron electrode. The surface of the copper plate was made round in order to fit the spherical bottom of the glass chamber.

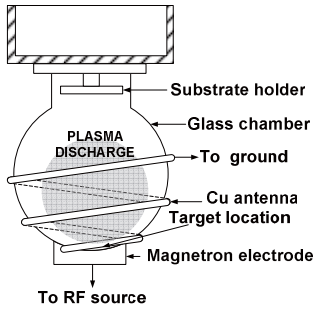

Figure 3. Details of the sputtering chamber in ICP mode.

chamber so as to reduce the capacitance of this part as will be described in the following section. The chamber was enclosed in a metallic cage in order to shield the RF field leakage.

Both inductive and capacitive coupling modes to the gas discharge were investigated. In the inductively coupled plasma (ICP) mode, inductive coupling to the plasma was accomplished by properly arranging the impedance of the circuit components. A 4-mm diameter Cu tube formed an antenna spirally wound around the chamber. The number of turns of the antenna changes the impedance which alters the RF amplitude across the antenna. One end of the antenna was connected to the electrode and RF power source while the other end was connected to ground. Figure 3 shows the details of the sputtering chamber in ICP mode.

In the capacitively coupled plasma (CCP) mode, capacitive coupling was achieved using different configurations. In one configuration, capacitive coupling to the gas discharge was achieved via a hot-tungsten assisted plasma ignition. Once the plasma was ignited by a tungsten filament, the RF power sustained the discharge with the filament turned off. In another configuration, capacitive coupling was accomplished by wrapping a 50-mm wide Cu sheet around the middle part of the chamber to serve as the counter electrode. A third configuration was investigated by inserting a 40-mm x 60-mm Cu plate inside the chamber to act as the counter electrode. Both counter electrodes in the two configurations were connected to ground. Figure 4 shows the schematic diagrams of the sputtering chamber in different CCP configurations.

A 99.9999% pure Ga was suspended upon the bottom of the chamber. Due to its low melting temperature, the Ga metal was in its liquid state in a plasma chamber operated at room temperature. Base pressures of 5.3 x 10^{-5} Pa and 2.4 x 10^{-4} Pa were achieved in the analysis and discharge chambers, respectively. Argon (Ar) and Nitrogen (N_2) were used as the operating gases with the pressure varied to study the spatial distribution of the produced plasma. A Quadrupole Mass Analyzer (QMA), SRS RGA200, which can determine atomic masses up to 200 amu, was installed in the analysis chamber directly above the orifice to determine sputtered Ga flux. An Optical Emission Spectrometer (OES), Ocean Optics HR4000, was used to monitor optical emissions between 380–470 nm of the different species present in the discharge. An optical fiber cable connected to the

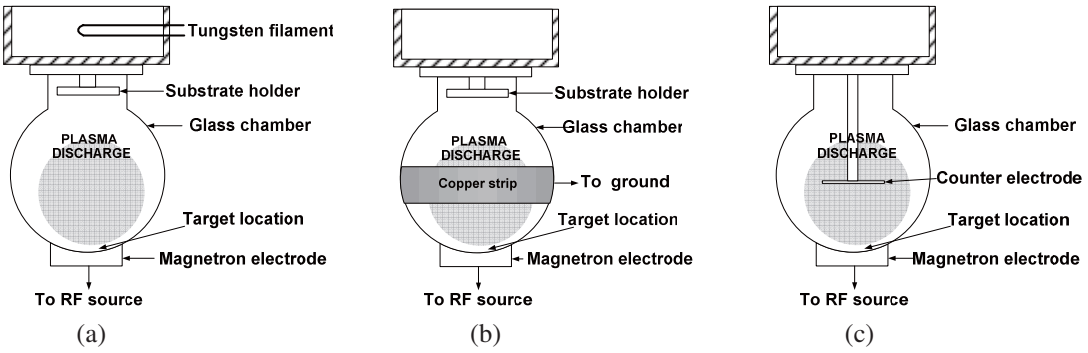

Figure 4. Details of the sputtering chamber in CCP mode. (a) hot tungsten assisted ignition; (b) the chamber with a Cu strip counter electrode; and (c) the chamber with an internal Cu plate counter electrode.

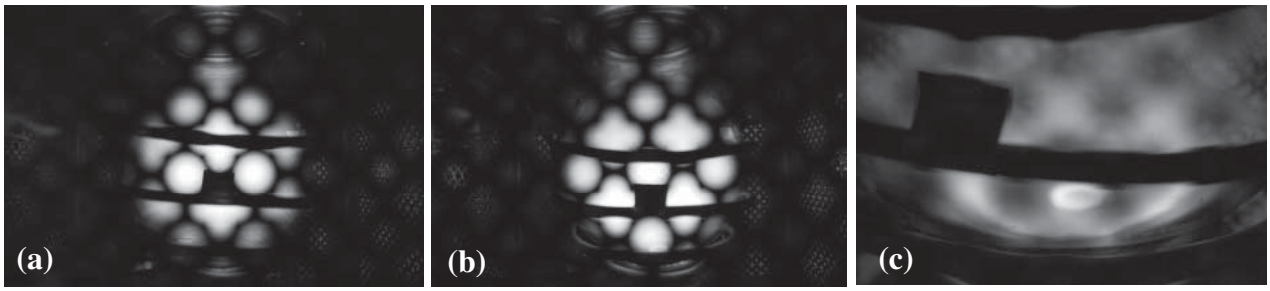

Figure 5. Ar plasma discharge (a) without the magnetron electrode; and (b) with magnetron electrode. (c) A close-up of the plasma discharge with the magnetron electrode near the vicinity of the target location.

entrance slit of the spectrometer was positioned in such a configuration that the line of sight passes through a point directly above the target surface.

3. Results and Discussions

3.1 *Magnetron Electrode*

The system was operated using an ordinary Cu electrode mounted at the bottom part of the glass chamber without magnets. When plasma was ignited, a homogeneous discharge was observed around the center of the chamber, as shown in Fig. 5(a). In this mode, sputtering of a target suspended on the chamber bottom was inefficient. With replacement to the magnetron electrode, plasma density was effectively increased and the dense discharge was confined at the bottom part of the chamber near the location of the target as shown in Fig. 5(b). The efficiency of the ionization process was increased by the presence of the magnetic field in the vicinity of the target surface thus enhancing the coupling between the discharge and the RF power source. A close-up view of the effect of the magnetron electrode on the discharge is shown in Fig. 5(c). The magnetic field successfully confined the discharge near the Ga target. Thus, the electron density in front of the Ga target is higher in a magnetron sputtering system compared to a simple diode sputtering system. Figure 6 shows the effect of the magnetron electrode in decreasing the power reflectance of the system compared to a diode sputtering system. Even with the presence of an insulating glass layer, the magnetron electrode is capable of improving the coupling efficiency of the power supplied to the discharge and sustaining stable discharges at higher RF powers.

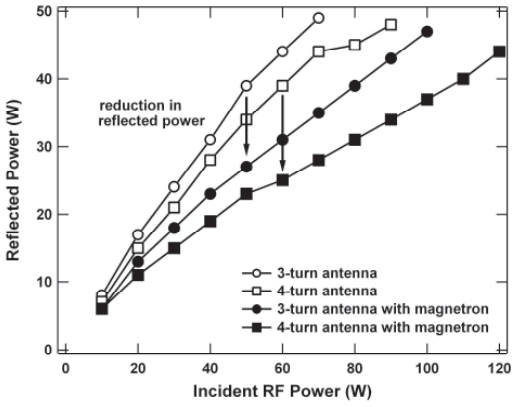

Figure 6. Comparison of the effect of the magnetron electrode in decreasing the reflected power.

3.2 *RF Power Coupling to the Discharge*

3.2.1 *Inductive Coupling Mode*

Coupling of the applied RF power to the discharge was accomplished in either inductive or capacitive mode. In the ICP mode, different turns of the Cu antenna were tested in order to tune the system to resonance. Two-turn, three-turn and four-turn antenna configurations were investigated with Ar as the operating gas with the pressure varied from 0.07 Pa to 13.3 Pa. Among these configurations, the three-turn antenna provided the smallest reflection below 125 W incident RF power while the two-turn antenna showed the lowest reflection beyond 125 W. The observed low reflectance corresponds to higher coupling of the antenna and efficient absorption of the supplied power to the gas discharge. Thus, the density of the plasma is higher in

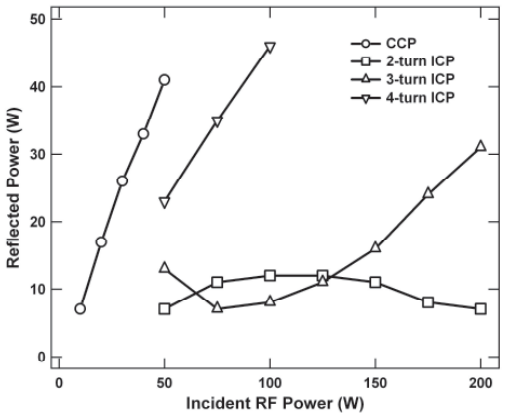

Figure 7. Comparison of reflected power with respect to RF incident power in ICP and CCP modes at 1.3 Pa Ar gas pressure.

this mode. Gas discharges were effectively sustained in the chamber beyond 200 W RF power with at most 15% reflection. Figure 7 shows a comparison of reflected power with respect to the incident power and different turns of the antenna. In addition, the figure also shows the difference between an ICP and CCP configuration in terms of reflected power and incident RF power.

3.2.2 *Capacitive Coupling Mode*

As for the CCP configuration, Ar plasma was sustained via a hot-tungsten assisted ignition. In this configuration, gas discharge was maintained up to 60 W with reflectance around 80%. The pressure of Ar gas was varied between 0.67 and 13.3 Pa. Plasma density was low in the above mentioned RF power and Ar pressure range. In a second configuration, a Cu metal strip was wrapped outside the middle part of the glass chamber to make it as the counter electrode. Also, in this configuration, plasma was sustained up to 60 W with 80% reflected power in the same RF power and Ar gas pressure range as in the previous configuration. The high reflectance can be attributed to the poor coupling of the RF power to the gas discharge. Thus, a third configuration was tested by placing a counter electrode inside the chamber. However, similar results were observed as in the two previous CCP configurations. A typical result of power reflectance measurements under the CCP mode is shown in Fig. 7 where high power reflectance can be observed at low RF powers. Poor coupling of the plasma to the discharge in these configurations can be ascribed to the 5 mm thickness of the insulating reservoir. The electrical charges that are accumulated on the glass surface affect the field strength of the discharge space thereby changing the breakdown voltage of the background gas.[5] Since the thickness of the dielectric (glass) layer is large, the resulting capacitance as small as 0.2 pF/cm^2 diminishes the amount of charge induced by the RF voltage.

Figure 8(a) shows a schematic of the system around the target while the equivalent electric circuit is shown in Fig. 8(b). The overall voltage across the plasma sheath and the glass reservoir is the sum of the voltage across the sheath and the voltage across the reservoir which can be represented as

$$V_{RF} = \frac{J_{RF}}{\omega C_{sheath}} + \frac{J_{RF}}{\omega C_{reservoir}} \qquad (1)$$

where V_{RF} is the RF voltage, ω is the RF frequency, J_{RF} is the current density which is constant across the sheath and the reservoir, C_{sheath} and $C_{reservoir}$ are the capacitance per unit area of the sheath and that of the reservoir, respectively. In a capacitive discharge, the effective capacitance per unit area, under the assumptions of time-independent, collisionless ion motion and inertialess

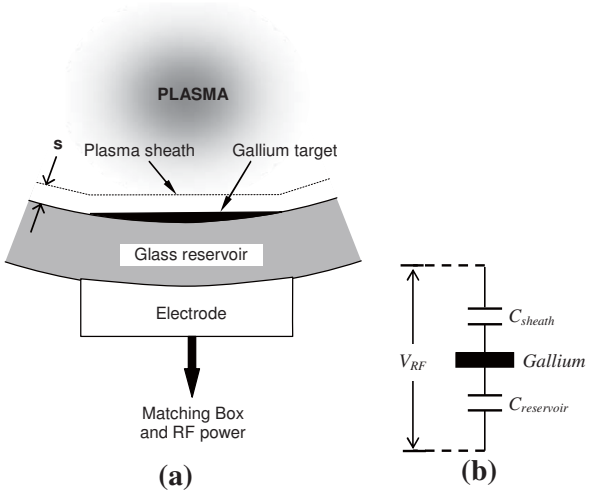

Figure 8. (a) Schematic representation of the arrangement of different components near the target location showing the magnetron electrode, glass reservoir, Ga target and the plasma sheath. (b) Electric circuit equivalent of the assembly.

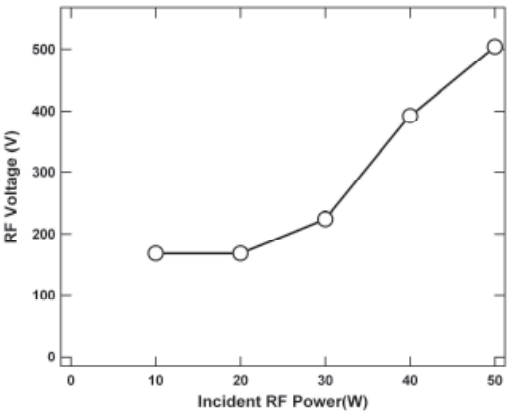

Figure 9. Variation in the RF voltage with respect to the RF power.

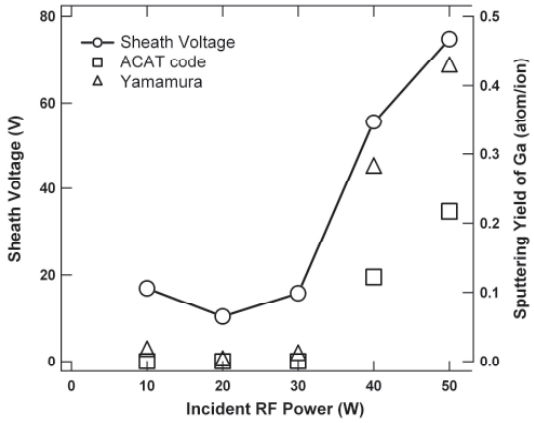

Figure 10. Variation in the sheath voltage with respect to the RF power and the computed sputtering yields from the Yamamura sputtering yield formula and ACAT code.

electrons in a high voltage, capacitive RF sheath driven by a sinusoidal current source, is defined, as proposed by Lieberman, [6] to be

$$C_{sheath} \approx 1.226 \frac{\varepsilon_0}{s} \tag{2}$$

where ε_0 is the permittivity of vacuum and s is the sheath thickness. Furthermore, the sheath thickness is dependent on the sheath voltage, V_{sheath}, which is calculated by[6]

$$s = \sqrt{0.82\varepsilon_0 \left(\frac{2e}{M}\right)^{1/2} \frac{V_{sheath}^{3/2}}{J_i}}\,. \tag{3}$$

Here, e is the elementary charge, M is the atomic mass of the ion and J_i is the DC ion current density. Equation (3) applies to a collisionless sheath which is valid at low pressure (long ion mean free path) and small Debye length (thin sheath). In addition, J_i is defined as

$$J_i = en_0 \sqrt{\frac{eT_e}{M}} \tag{4}$$

where n_0 is the plasma density and T_e is the electron temperature. In the experimental conditions, n_0 was in the range of 10^{10} cm^{-3} and increased linearly with RF power while T_e ranged from 3 to 4 eV.

The effective capacitance per unit area of the insulating reservoir can be determined from

$$C_{reservoir} = \frac{\varepsilon_r \varepsilon_0}{d} \tag{5}$$

where ε_r is the relative permittivity of the glass taken to be 4.6 and d is the thickness of the insulating layer which is 0.005 m.

From Eqs. (1)-(5), the voltage across the sheath can be expressed as

$$V_{sheath} = \frac{V_{RF}}{\left(1 + \frac{C_{sheath}}{C_{reservoir}}\right)} \tag{6}$$

Figure 9 shows the dependence of the RF voltage with respect to the applied RF power. As the RF power increased, the RF voltage also increases. Without the presence of an insulating layer, the potential across the sheath and the magnetron electrode is the RF voltage. This is the bias induced on a target placed on the top of the magnetron electrode. However, when an insulating layer is inserted between the discharge and the magnetron electrode, the bulk plasma induces a self-bias on the sheath. Using Eq. (6), the variation in the voltage across the sheath and the applied RF power can be computed. Figure 10 shows the variation in the sheath voltage with respect to the RF power in a system with an insulating layer. A significant decrease in the induced sheath voltage can be observed. Thus, the presence of the insulating surface caused smaller RF self-bias in the CCP mode. The low self-bias voltage induced on a sheath affects the sputtering efficiency when a target is placed on the insulating layer. In addition, an insulating layer between an electrode and the discharge reduces the RF power coupling efficiency. This consequence can be seen in Fig. 7 where high power reflectance was observed when the system was operated in CCP mode.

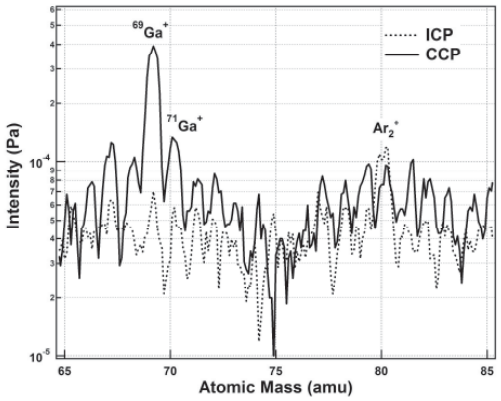

Figure 11. Mass spectra of Ar discharge with Ga target at 50 W incident RF power and 0.67 Pa gas pressure.

When an ion traverses a plasma sheath having a potential V_{sheath}, the ion will acquire an energy equivalent to eV_{sheath}, which becomes the bombarding energy incident on a target surface. With a known incident energy, the sputtering yield can be approximately obtained using the semi-empirical Yamamura sputtering yield formula[7] and the Monte Carlo simulation code ACAT (Atomic Collisions in Amorphous Targets)[8] which is based on binary collision approximation. The surface binding energy of Ga is set to 2.81 eV and the threshold energy is 12.94 eV. Shown in Fig. 10 are the sputtering yields of Ga bombarded by Ar ions using the Yamamura sputtering yield formula and ACAT. Both cases predicted that at very low at RF powers (<30 W), the sputtering yield is negligible. As the RF power increases, the sputtering yield also increases. Thus, at around 50 W RF power in the CCP mode, sputtering of Ga in Ar plasma can be observed. Based on these predictions, even at sheath potentials less than 100 V, sizable sputtering yield of Ga is present. The sputtered particles may have enough energy to traverse the sputtering chamber and be detected by the QMA.

3.3 *Liquid Gallium Target Irradiation*

In both the ICP and CCP configurations, the Ga target was irradiated with Ar and N_2 plasmas separately. In the ICP case, mass spectral analyses revealed minute amounts of Ga ion current in the analysis chamber as compared to the CCP case where Ga ions were observed. The minimal presence of sputtered Ga species in the analysis chamber in the ICP mode suggests that the bombarding energies of the ions may not be enough to eject Ga atoms from the target surface. Low ion bombarding energy is typically observed in high density ICP systems[9]. However, in the CCP mode, even at low RF powers and high system reflectance, bombarding ions have enough energy to sputter out target atoms, thus Ga species were observed in the analysis chamber. The mass spectra under Ar plasma with Ga target from both configurations are shown in Fig. 11. A comparison of the Ga mass spectral intensities showed an increase with increasing gas pressure and increasing RF power under pure Ar plasma irradiation. However, in pure N_2 plasma, the mass spectral intensities of Ga decrease with increasing gas pressure while it increases with increasing RF power. The decrease in intensity of the Ga line under

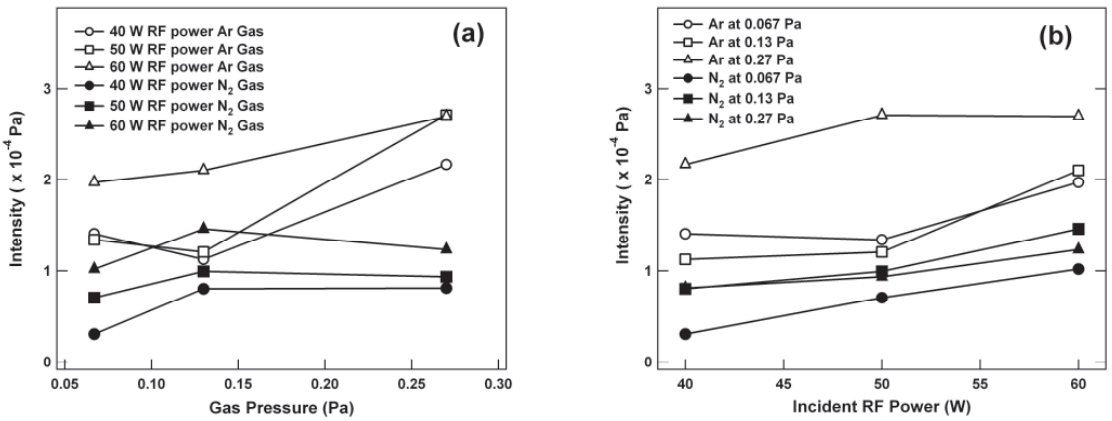

Figure 12. Comparisons of the Ga flux intensities measured by a QMA to (a) gas pressure, and that to (b) incident RF power.

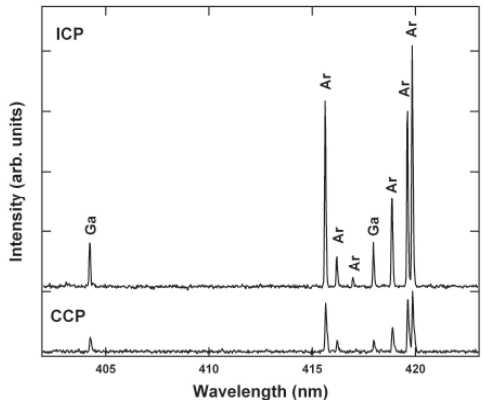

Figure 13. Optical emission spectra of Ar discharge with Ga target at 50 W incident RF power in ICP and CCP modes.

pure N_2 plasma can be attributed to the passivation of the target surface with GaN. The passivation of the Ga target surface with GaN had been observed under pure N_2 irradiation.[3] Passivation is an unwanted phenomenon since it decreases the sputtering efficiency thus adequate self-biasing on the target surface by the gas discharge is necessary. The comparisons of Ga mass spectral intensities are shown in Figs. 12(a) and 12(b).

Optical emission spectral analyses revealed the presence of different species in the discharge in both the ICP and CCP configurations. This implied the ionization of different elements as well as the target atoms near the target surface. Figure 13 shows typical optical emission spectra of the discharge near the target surface. Ga spectral line intensities are higher in ICP mode compared to CCP mode. The high intensity of the spectral lines corresponds to high plasma density in the ICP mode as compared to the low plasma density in the CCP mode, when electron temperature is nearly constant. However, this observation contradicts the mass spectral analyses of the two modes of operation. This means, even though Ga emission lines were observed, the energy of the sputtered Ga species in ICP mode may not be enough to traverse the analysis chamber. This suggests that Ga atoms are liberated from the Ga surface by evaporation process. In the CCP mode, although the emission lines were small, the sputtered Ga species may have gained enough energy to traverse the analysis chamber as they are produced by sputtering and be detected in the QMA.

3.4 *Electron Temperature*

When plasma is assumed to be in local thermodynamic equilibrium (LTE), the electron temperature (T_e) of the gas discharge can be determined from the relative intensities between two spectral lines corresponding to the transition of different energy levels. In order to compare T_e of ICP and CCP discharges without disturbing the plasma inside the chamber, T_e of both configurations were estimated using the LTE approach by taking into account the transition of electrons from an upper level n to a lower level m using the relation

$$\ln\left(\frac{I_{nm}\lambda_{nm}}{g_n A_{nm}}\right) = -\frac{\Delta E_n}{kT_e} + C \qquad (7)$$

where I_{nm} is the intensity of the line spectrum emission, λ_{nm} is the wavelength of the spectral line, g_n is the statistical weight of the upper energy level n and A_{nm} is the atomic transition probability. ΔE_n is the excitation of upper level n, k is the Boltzmann constant and C is a constant. The data for Ar spectrum line parameters were taken from NIST[10] database. In order to use Eq. (7), one has to know the absolute intensity of the emission line which can be affected by several factors making it difficult to accurately determine T_e. Thus, to obtain T_e approximately, a pair of emission lines emitted by the same species with a large difference in excited energies was used. Using Eq. (7) for each spectral line and combining the two equations, leads to

$$T_e = \frac{E_2 - E_1}{k}\left[\ln\left(\frac{I_1\lambda_1 g_2 A_2}{I_2\lambda_2 g_1 A_1}\right)\right]^{-1} \qquad (8)$$

where the subscripts 1 and 2 denote the first and second spectral lines under consideration, respectively.

A cursory check of T_e of an Ar gas discharge was performed using the LTE approach. Using the intensities

of the 425.93 nm ($3s^2 3p^5(^2P°_{1/2})4s$ - $3s^2 3p^5(^2P°_{1/2})5p$) and 434.80 nm ($3s^2 3p^4(^3P)4s$ - $3s^2 3p^4(^3P)4p$) spectral lines of Ar, T_e were computed using Eq. (8) from the gas discharge in CCP and ICP configurations. As shown in Fig. 14, T_e of an ICP discharge is lower compared to a CCP discharge at 50 W RF power and with Ar gas pressure varied from 0.40 Pa to 1.33 Pa. Due to the oversimplification of the LTE approach and the large deviation from the equilibrium state of the discharges, the computed T_e may differ significantly from the actual electron temperatures in the discharge. But in terms of relative values, T_e in a CCP discharge is higher than that of an ICP discharge as revealed by the computations above.

The low T_e in ICP translates to low plasma potential which leads to low sputtering yield even with low system reflectance. On the other hand, CCP configuration provided high T_e even with low power absorbance. Following Lieberman's assumption that ions enter the RF sheath with a Bohm presheath velocity, u_B[6)]

$$u_B = \sqrt{\frac{eT_e}{M}} \tag{9}$$

it follows that higher T_e is desirable in order to increase the energy of the ions entering the sheath and thereby enhance the sputtering efficiency of a target material. Since the CCP configuration offers higher electron temperature compared to ICP configuration this would lead to an increase in the sputtering efficiency of the liquid target material. However, due to the insulating nature of the reservoir, high power reflectance was observed which limited the operation of the system at higher RF powers. Even with limited RF powers, directional sputtering can be effective in the CCP configuration compared to the ICP configuration. Nevertheless, as elucidated in the previous section, the sputtered species in CCP mode may have gained enough energy because of the high energy ions bombarding the surface due to higher T_e.

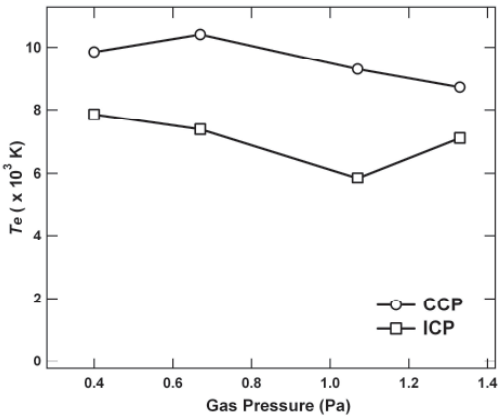

Figure 14. Electron temperature of Ar gas discharge at 50 W incident RF power as estimated by using the LTE approach.

4. Conclusions and Future Directions

A RF sputtering system with an insulating reservoir has been tested using different coupling modes. A planar magnetron electrode was designed and mounted to an insulating reservoir which contributed to the decrease in system reflection, sustain stable discharges at higher incident powers and confine a homogeneous region of the discharge within the vicinity of the liquid metal target located far from the location of a deposition substrate. Confinement of the discharge near the target location enhances the interaction between the discharge and the target surface. The inductive system exhibited good coupling, high plasma density at high RF powers and small reflectance. However, mass spectral analyses did not confirm significant presence of sputtered Ga atoms in the analysis chamber. This suggests that the ion bombarding energy in ICP mode may not be enough to sputter Ga atoms with higher energies capable of reaching the analysis chamber.

In the capacitive coupling mode, the insulating nature of the glass reservoir hindered the effective transmittance of the RF power to the gas discharge which led to poor coupling. Thus, the CCP system exhibited high power reflectance and limited the operating RF power. However, even at low RF powers, the CCP configuration was capable of sputtering a liquid Ga target as confirmed from

the mass spectral analyses. Theoretical sputtering yield calculations revealed that even with low sheath potential, the CCP configuration is able to sputter Ga under Ar plasma.

Comparison of T_e under LTE approximation from the two coupling configurations showed that in the ICP mode, T_e is lower compared to the CCP mode. Low T_e leads to low ion saturation current which reduces the sputtering efficiency of the target. In the CCP case, even at low RF powers, high T_e was observed which enhances the sputtering efficiency of Ga target.

The present experimental apparatus was able to demonstrate the sputtering of liquid metal target like Ga with the presence of an insulating reservoir. However, in order to improve coupling efficiency of the gas discharge to the RF power in CCP mode, the thickness of the glass chamber should be reduced. In addition, dual frequency operation may be employed in order to separately control plasma density and ion energy. Utilizing a conductive yet chemically inert target holder is being examined. Exploring other means of plasma excitation like electron cyclotron resonance is also a possibility.

5. Acknowledgements

This work was supported by the High Tech Research Center Project, “Interfacial Science”, at Doshisha University. One of the authors, M. V. Jr. thanks Harris Science School Foundation Grant from Doshisha University.

6. References

1) W. Hitchon, *Plasma Processes for Semiconductor Fabrication* (Cambridge Univ. Press, New York, 1999) p. 8.
2) T. Shiosaki, S. Ohnishi, Y. Murakami and A. Kawabata, “High rate epitaxial growth of ZnO films on sapphire by planar magnetron rf sputtering system,” J.Cryst. Growth, **45,** 346-349 (1978).
3) R. Flauta, M. Vasquez, Jr., H. Ramos and M. Wada, “Effect of Surface and Growth Conditions for Formation of Textured Polycrystalline GaN Crystals by Reactive N_2 Plasma,” Jpn. J. Appl. Phys. Part 1 **45** 8512–8516 (2006).
4) T. Kikuma, K. Tominaga, K. Furutani, K. Kusaka, T. Hanabusa and T. Mukai, “GaN films deposited by planar magnetron sputtering,” Vacuum **66** 233 – 237 (2002).
5) M. Shoji and M. Sato, “Argon gas breakdown with bare and insulated electrodes in dc-biased RF field,” J. Phys. D.: Appl. Phys. **32** 1640 – 1645 (1999).
6) M. A. Lieberman, “Analytical Solution for Capacitive RF sheath, ” IEEE Trans. Plasma Sci., **16** 638 – 644 (1988).
7) Y. Yamamura and H. Tawara, “Energy Dependence Of Ion-Induced Sputtering Yields From Monatomic Solids At Normal Incidence,” Atomic Data and Nuclear Tables, **62** 149 – 253 (1996).
8) Y. Yamamura and Y. Mizuno, IPPJ-AM-40, Inst. Plasma Physics Nagoya Univ. (1985).
9) M. A. Lieberman and A. J. Lichtenberg, *Principles of Plasma Discharges and Materials Processing* (Wiley, New York, 1994) p. 309.
10) Y. Ralchenko, A. E. Kramida, J. Reader and NIST ASD Team (2008). NIST Atomic Spectra Database (version 3.1.5), [Online]. Available: http://physics.nist.gov/asd3 [2008, September 13]. National Institute of Standards and Technology, Gaithersburg, MD.